Relative sea-level sensitivity in the Eurasian region to Earth and ice-sheet model uncertainty during the Last Interglacial

Oliver G. Pollard [a,*], Natasha L.M. Barlow [a], Lauren J. Gregoire [a], Natalya Gomez [b]

[a] *School of Earth and Environment, University of Leeds, Leeds, UK*
[b] *Department of Earth and Planetary Sciences, McGill University, Montreal, QC, Canada*

ARTICLE INFO

ABSTRACT

Fingerprinting the source and rate of the melt of polar ice sheets during the Last Interglacial is a key research challenge. This is reliant on high-quality relative sea-level constraints, and the correction of this data for the effects of glacial isostatic adjustment driven by ice sheet cover changes prior to the interglacial. However, both the spatial and temporal evolution of past ice sheets and the Earth's rheological structure that serve as inputs to glacial isostatic adjustment predictions are significantly uncertain. This study sets out to determine the relative influence of each of these inputs on modelled values of Last Interglacial relative sea levels and how this influence varies spatially. To answer this question, we use a palaeo ice-sheet model and a gravitationally consistent glacial isostatic adjustment model. We develop new numerical tools to generate plausible ice-sheet extent and histories, quantify relative sea-level uncertainty, and perform a Sobol sensitivity analysis facilitated by the use of Gaussian process emulation. We find that Earth model parameters are the dominant contributors to relative sea-level uncertainty in most Eurasian regions, but that relative sea-level values in the Barents-Kara Sea are most influenced by ice-sheet loading, while the timing of the deglaciation has the greatest impact in the Baltic Sea. Our results show that the magnitude and rate of relative sea-level change is relatively insensitive to the specific timing of ice-sheet retreat, as well as the configuration of the far-field North American ice sheet. Overall, our work suggests that the coastlines of the southern North Sea and the English Channel are least influenced by relative sea-level uncertainty and are the most suitable for future data collection studies aiming to limit the influence of glacial isostatic adjustment.

1. Introduction

The LIG (MIS 5e; 130–116 ka) was the last time in Earth's history that the Greenland and Antarctic ice sheets were smaller than those of today (Capron et al., 2014; Otto-Bliesner et al., 2006). Assessing the rate, timing, and pattern of ice-sheet retreat during this period may shed light on possible future ice-sheet evolution in response to increased polar temperatures and help to constrain the pattern and rate of global sea-level change on multi-century to millennial timescales (IPCC, 2022). A significant source of uncertainty in long-term future projections is the rate and magnitude of sea-level rise caused by the melt of the Antarctic Ice Sheet (Kopp et al., 2017; Turner et al., 2023), and therefore identifying the contribution of the Antarctic Ice Sheet to LIG global mean sea level is important. Due to its location, the pattern of LIG RSL (defined as the difference in sea surface elevation relative to the solid surface, compared to modern day) in some northwest Eurasian regions (Fig. 1A) is sensitive to the evolution of the interglacial Antarctic Ice Sheet (Fig. 1B), but relatively insensitive to the melt of the

Greenland Ice Sheet (Hay et al., 2014; Mitrovica et al., 2011; Clark and Lingle, 1977), and could therefore be used to identify sources of LIG ice-sheet melt. In addition, some regions within northwest Eurasia, such as the North Sea, contain valuable sedimentary archives in which these past sea-level changes are recorded (Cohen et al., 2022; Zagwijn, 1983). However, such geological records reflect the cumulative contribution of multiple geophysical processes that must be quantified if they are to be used to isolate the fingerprint of LIG Greenland and Antarctic Ice Sheet melt (Hay et al., 2014; Dendy et al., 2017).

RSL changes throughout interglacial periods are driven by both the contribution of ice-sheet melt that occurred during the same interglacial, as well as the ongoing influence of GIA from ice-sheet mass changes that occurred in the glacial periods prior (Lambeck et al., 2012). In regions that are in the vicinity of former ice sheets, such as Eurasia, the contribution of ongoing GIA from previous glacial cycles to the interglacial RSL signal is significant and adds complexity to fingerprinting ice-sheet melt (Hay et al., 2014; Dendy et al., 2017). As a result, research aiming to identify the sources of LIG ice-sheet
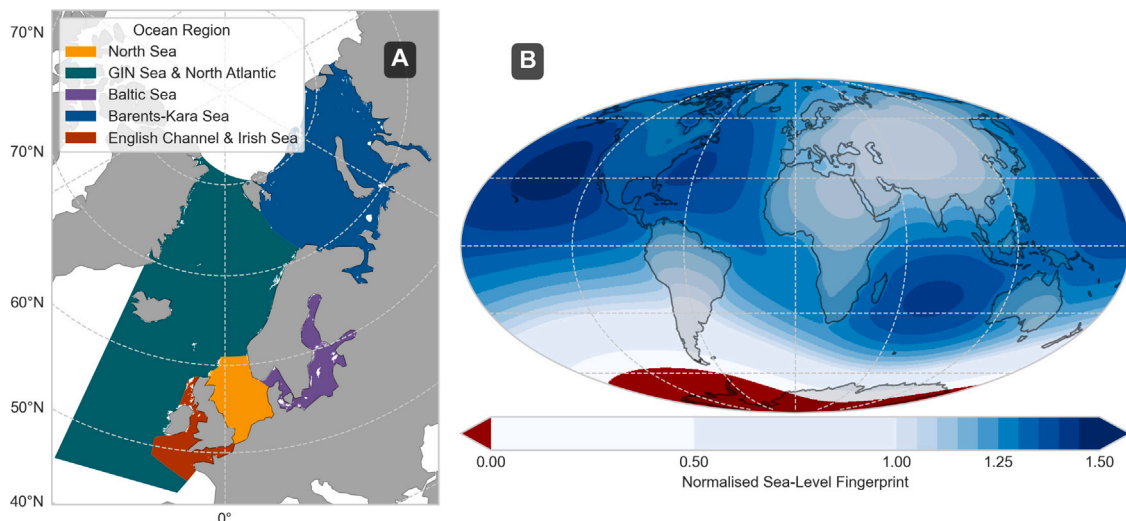

Fig. 1. Eurasian Study Site and the Antarctic Fingerprint. (A) Northwest Eurasian Ocean regional divisions that are used in this work. (B) Illustrative Antarctic sea-level fingerprint showing a prediction of the sea level change resulting from a complete collapse of the WAIS, normalised by the global mean sea level equivalent of the ice loss (5 metres in this scenario).

melt has largely focused on using RSL data from locations distal to Quaternary ice sheets (*e.g.* Bahamas, Western Australia) (Dutton et al., 2015; Dyer et al., 2021; O'Leary et al., 2013). However, Holocene studies in locations close to or beneath former ice sheets have shown that the development of regional, near-field GIA models, driven by ice-mass changes during the preceding Last Glacial Period (c. 25 ka), is an effective technique for the recovery of sea-level fingerprints from geological observations of RSL (Lin et al., 2021). Recent work by Barnett et al. (2023) has shown promise in identifying the timing of LIG ice sheet melt from near-field records. To do this, we must quantify and remove the GIA signal from near-field records in order to utilise them for understanding interglacial ice-mass changes (Barnett et al., 2023; Dutton et al., 2015; Dyer et al., 2021).

GIA is the term used to describe the changes in RSL and topography driven by surface ice-mass changes accounting for the influences of gravitational attraction, Earth rotation, and viscoelastic deformation (Farrell and Clark, 1976; Mitrovica et al., 2001; Peltier, 1974). Model predictions of GIA are dependent on the particular combination of the global ice-sheet history and viscoelastic Earth model used, yet both the configuration of global ice-sheet mass changes during glacial–interglacial cycles prior to the Last Glacial Period, including the Penultimate Glacial Period (ca. 200–130 ka, correlated to MIS 6), and the rheological structure of the solid Earth are highly uncertain. Ice-sheet changes during the Penultimate Glacial Period play a key role in determining the LIG near-field GIA simulation, making the application of GIA models to fingerprinting LIG ice-sheet melt a significant challenge (Dendy et al., 2017; Lambeck et al., 2014; Rohling et al., 2017). Previous studies of LIG GIA have approached this problem by testing a limited series of discrete, hand-picked scenarios for ice evolution and Earth model parameters which do not allow for the systematic assessment of GIA model sensitivity and uncertainty (Dendy et al., 2017; Dyer et al., 2021). In addition, the choice of ice-sheet history and Earth model is often tuned to LIG RSL databases, creating a circularity issue when extracting fingerprints from the same datasets.

Here we develop a new methodology to enable a full systematic assessment of RSL variability due to uncertainties in the ice-sheet evolution and viscoelastic Earth structure that drive modelled LIG RSL changes, independent of sea-level data. In addition, building upon work by Pollard et al. (2023), we explore the uncertainty in the evolution of the EIS during the Penultimate Glacial Period, which is of particular importance to GIA in the North Sea and wider Eurasian region. Finally,

we apply sensitivity analysis to our large ensemble of GIA model outputs to decompose the RSL variability into the relative contributions from each parameter, thus revealing spatial patterns of sensitivity to help guide site-specific studies on the most critical sources of RSL uncertainty.

2. Methods

We designed and implemented a state-of-the-art workflow to evaluate uncertainties in LIG sea-level evolution due to past ice load and solid-Earth structure. Our workflow, depicted in Fig. 4, combines (i) a process for generating an ensemble of plausible Eurasian ice-sheet histories that uses a simple ice-sheet model (Section 2.2) (ii) scenarios for the evolution of other ice sheets, including the Antarctic ice sheet (Sections 2.1.3–2.2.2), (iii) new tools to sample through uncertainty in the Earth structure and (iv) a gravitationally consistent sea-level model (Section 2.2.1). With this workflow, we ran ensembles of simulations of the sea-level model that efficiently sample through the uncertainty in ice-sheet history and solid-Earth parameters. We then conducted a Sobol sensitivity analysis on our ensemble of simulations to determine the relative sensitivity of LIG sea level to each uncertain input.

2.1. Modelling the Eurasian ice sheet during the Penultimate Deglaciation

The proximity of northwest Eurasian coastlines to the expansive Penultimate Glacial Period EIS means that the archives of LIG RSL are likely to be especially sensitive to mass balance changes of the EIS during the Penultimate Deglaciation (Long et al., 2015). However, little is known of the ice sheet's spatiotemporal evolution during this time, with previous ice-sheet modelling work typically focusing on its maximum extent or with significant uncertainty in the ice margin position (Batchelor et al., 2019; Colleoni et al., 2016; Lambeck et al., 2006; Svendsen et al., 2004; Pollard et al., 2023). We identify three types of uncertainty in characterising the deglaciation of the penultimate EIS: the maximum ice-sheet volume at the PGM; asynchrony in the pattern of the deglaciation (*e.g.* the eastern margin experiencing maximum extent at a different time to the west); and the rate and timing of ice retreat Toucanne et al. (2009), Ehlers et al. (2011), Ehlers and Gibbard (2004). In order to account for each of these sources of uncertainty within our uncertainty quantification, we perform dedicated numerical modelling of the EIS complex during the Penultimate Deglaciation. This builds upon and extends the work of Pollard et al. (2023), who solely focused on modelling the maximum ice-sheet extent.
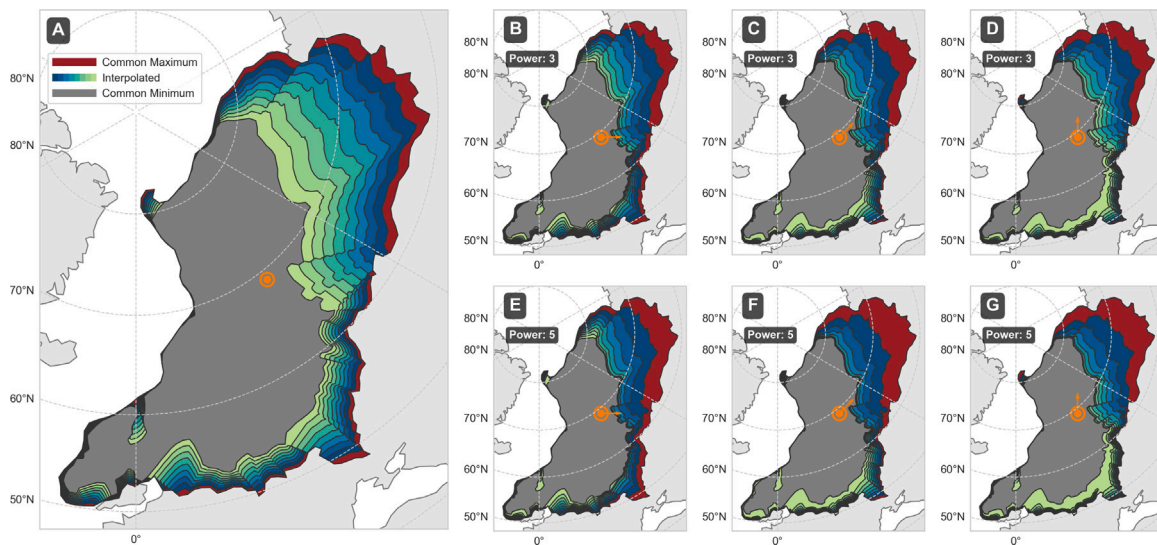
Fig. 2. Interpolated Penultimate Deglaciation Margins. (A) 7 intermediary margins between the common maximum (Batchelor et al. (2019) MIS 6 best-estimate) and common minimum (Hughes et al. (2016) LGM) extents are generated with a margin interpolation regime. (B-D) This scheme is able to generate asynchronously deglaciating margin series by specifying the angle of maximum asynchrony (orange arrow) and magnitude of asynchrony (power). (E-G) Same as (B-D) but with a greater magnitude of asynchrony power.

2.1.1. Ice-sheet model

We generate ice-sheet geometries using ICESHEET: a simple, steady-state ice-sheet model that assumes a perfectly plastic ice-sheet rheology (Gowan et al., 2016), and which has previously been utilised to generate ice-sheet reconstructions independently of sea-level and vertical land motion proxy data (Bradley et al., 2023; Gowan et al., 2021). The surface elevation is calculated assuming that the ice sheet is flowing like a perfectly plastic material in a steady state. Thus, the model neglects the effects of internal stresses, surface mass balance, and temporal evolution. The model does not have a regular grid-like thermodynamic ice sheet models. Instead, it iteratively resolved thickness along flowlines at regular intervals (here set at 5000 m) within prescribed ice sheet margins. The purpose of this simple model is not to attempt to solve ice velocity but simply to provide an approximation for the shape of ice sheets given its ice sheet margin and bedrock topography for use in a sea level or climate model.

ICESHEET takes three inputs in order to produce a single, time-independent ice geometry: a basal shear stress map, composed of a mosaic of categorised sediment regions and parameterised by sedimentary shear stress and the influences of basal conditions (detailed in Pollard et al. (2023)); regional topography, iteratively generated using a simple topographic deformation model; and prescribed ice-sheet margin. Pollard et al. (2023) has demonstrated that the simulated ice thickness can be calibrated to reconstructions or to dynamical ice sheets that account for the effects of ice dynamics, surface mass balance and the out-of-equilibrium state of the ice sheet at a given time. By varying the values within the 2D basal shear stress input, ensembles of ice sheet geometries matching deglacial Eurasian ice sheet reconstructions can be produced.

Here, our methodology utilises ICESHEET to assess uncertainty in (i) EIS volume, which is explored through testing a range of shear-stress values influencing ice thickness, (ii) margin retreat asynchrony, for which we have developed a methodology for generating series of possible margin deglaciation scenarios, described in the following section, and (iii) ice-sheet deglaciation timing.

2.1.2. Deglaciation margins

The ICESHEET model is time-independent, meaning that it takes a single prescribed margin as input and produces a single corresponding ice geometry as output, without advancing time or evolving margin position during the course of a model simulation (Gowan et al., 2016).

Therefore, in order to generate a series of deglaciating EIS geometries for the Penultimate Glacial Period using ICESHEET, we require a prescribed series of corresponding deglaciating ice-sheet margins. To do this, we first assume that the most extensive (maximum) ice-sheet position was the MIS 6 best-estimate ice-sheet margin from Batchelor et al. (2019) which likely corresponds to the large Drenthe substage (ca. 175–160 ka) of the Penultimate Glacial Period (Toucanne et al., 2009), as modelled in Pollard et al. (2023). We also assume for extents less than or equal to the LGM the ice sheet retreat in a similar way to that during the Last Deglaciation (Hughes et al., 2016) (maximum LGM ice extent shown in grey in Fig. 2). To bridge the gap between the MIS 6 Batchelor and LGM Hughes margins, given the very limited spatial–temporal constraints (as documented by Rohling et al. (2017)), we develop a margin interpolation algorithm named *ShaPy* which we use to generate 7 additional intermediary margins (Fig. 2a). Since each margin is subsequently used as input to the full ICESHEET ensemble, we choose to sample 7 ice-sheet margins in order to balance computational requirements and density of spatial coverage between the original bounding ice-sheet configurations.

Our interpolation regime allowed us to generate an arbitrary number of intermediary deglaciation margins. However, each margin was subsequently used as input to the full ICESHEET ensemble, resulting in 1064 ice-sheet model executions (532 input combinations, and 1 iteration). Therefore, the choice of 7 margins allowed us to strike a balance between the density of spatial sampling and computational requirements.

Geological records of the deglaciation of the EIS indicate that its pattern of retreat was likely asynchronous, with the eastern sectors deglaciating earlier than the west (Patton et al., 2017). We therefore explore the impacts of deglacial asynchrony on RSL within this interpolation regime through the introduction of two parameters: async angle A_θ, which controls the direction of maximum asynchrony; and async power A_n, which determines the magnitude of asynchrony. A value of $A_n = 1$ corresponds to no asynchrony (Fig. 2a) and renders the value of A_θ obsolete. We set the A_θ value range, expressed in radians, to between π–1.5π relative to the projected y-axis, spanning the full Eastern margin from the edge of the Barents-Kara Sea (π) to the beginning of the southern-European margin (1.5π), while A_n ranges from between 1–5 (Fig. 2).

2.1.3. Ensemble design

The ICESHEET model requires the input of a basal shear stress map. To sample the uncertainty in this two-dimensional input, Pollard et al. (2023) parameterised the sheer stress map using 9 parameters that control regional shear-stress values as well as the influence of basal sliding and cold-based ice (Pollard et al., 2023). The parameter values are kept constant through time for simplicity. Some parameters apply to regions that relate to the distance from the margin, thus for a given set of parameter values we obtain one sheer stress map for each margin we model. We initially generate a 1200-member Latin Hypercube Sampling of the 9 shear-stress parameters and 2 margin asynchrony parameters. Since there is no observational evidence available to constrain ice-sheet thickness during the Penultimate Deglaciation, we employ a modelling approach where each parameter sample is first used to simulate EIS configurations during the Last Deglaciation. The ability of each combination to match ice-sheet reconstructions during the Last Deglaciation is quantified with an implausibility value Pollard et al. (2023) and we exclude simulations that fall outside of an implausibility criteria of 3-sigma, ruling out 668 of the parameter combinations as implausible and leaving 532 remaining combinations to evaluate during the Penultimate Deglaciation. Each asynchrony value pair is processed by the ice-margin interpolation algorithm to produce 532 corresponding ice-margin series. In turn, each margin series is used as input to ICESHEET, in combination with the corresponding shear stress map configuration, to generate 532 series of ice-sheet deglaciation geometries.

In order to approximate the effects of topography deformation from ice-sheet loading we input the initial ensemble of ice-sheet thickness outputs, along with the modern-day topography, into the fully relaxed form of the simple Elastic Lithosphere Relaxing Asthenosphere (ELRA) deformation model, assuming a bedrock density of 3300 kg m^3 and lithospheric flexural rigidity of 10^{25} N m (Coulon et al., 2021). This simple approach allows us to account for the first order effects of deformation on ice thickness without having an ordered time history of ice loading at this stage in the process. We do not expect that varying the Earth model treatment would significantly impact the range of ice volumes in our ensemble since the latter is significantly more sensitive to the choice of basal friction coefficient. We do, however, consider a full range of Earth model parameters when computing relative sea level during the LIG with a more sophisticated glacial isostatic adjustment model at a later stage in our analysis (see Section 2.2). The resulting ensemble of deformed topographies is used to perform an iteration of the ICESHEET ensemble, producing our final ensemble of deglaciation geometries (as was done in Pollard et al. (2023) for the PGM ice-sheet configurations). Each series of ice-sheet geometries is ordered from PGM to fully deglaciated, but the absolute timing of each configuration is not yet fixed. We then test a range of possible rates and timings of ice-sheet retreat using these modelled geometries (detailed below).

2.1.4. Eurasian ice sheet simulation results

Our ensemble has a PGM volume of 53 ± 7 m (mean $\pm$ 1 standard deviation) sea-level equivalent (SLE) (defined as the resulting global mean sea-level change that would result from evenly distributing the ice-sheet volume across modern-day ocean area). The Barents-Kara Sea ice-sheet region holds the largest amount of ice by volume at 28 ± 4 m SLE, followed by Fennoscandia at 24 ± 3 m SLE and the British-Irish ice sheet at 1.8 ± 0.1 m SLE. As the deglaciation progresses, the Barents-Kara Sea experiences the largest loss of volume, shrinking by 25 ± 7 m SLE between the invariant PGM and LGM margin positions. The Fennoscandian region has the largest average volume for all margins except for the PGM, losing only 10 ± 7 m SLE between the PGM and LGM. Over the full ensemble, the thickness of the eastern ice-sheet margin can be seen to rapidly diminish, and this is, in part, due to the presence of ensemble members with less extensive margins (larger A_n values). This also results in a relatively high thickness standard deviation of 0.8 km in this region.

In order to reduce the dimensionality of our model parameter space for subsequent analysis, we choose to analyse model sensitivity to regional ice-sheet volume values at the PGM only, rather than for each margin configuration. This simplification is based on the assumption that an ensemble member with a particularly large ice-sheet volume at the PGM configuration will also have a similarly large ice-sheet volume for all deglaciation subsequent configurations, relative to the other ensemble members. To test this assumption, we first express our ensemble of regional volume values in terms of standard deviations from the mean in order to quantify the relative position of each member within a particular margin volume distribution. By analysing the change in this position throughout the deglaciation, we find that the position of each member changes, on average, by 0.52, 0.33, and 0.30 standard deviations for the Barents-Kara Sea, Fennoscandian, and British-Irish regions, and these low values indicate that this a reasonable assumption.

2.2. Modelling relative sea level during the last interglacial

Our new EIS deglaciation geometries, which address uncertainties in deglaciation asynchrony and ice-sheet volume, must now be combined with a global ice-sheet history and rheological Earth model as inputs to a GIA model, in order to calculate the resulting RSL ensemble and associated sensitivities. To do this, we use a numerical GIA model combined with global-ice sheet scaling and Earth model generation algorithms to test value ranges for parameters describing the deglaciation timing, Northern hemispheric ice-sheet volume, and Earth model uncertainties.

2.2.1. Glacial isostatic adjustment model

We utilise a global GIA model to solve the Sea-Level Equation up to spherical harmonic degree and order 512, following the pseudo-spectral implementation by Kendall et al. (2005). Output in the spatial domain is produced on a 512×1024 Gauss–Legendre lat-long grid (hereafter referred to as the model grid). We assume a 1D Maxwell viscoelastic Earth structure with elastic characteristics determined by the Preliminary Reference Earth Model (PREM) (Dziewonski and Anderson, 1981) and a simple, step-wise viscosity profile, following previous GIA modelling efforts (*e.g.* Bradley et al., 2023; Dendy et al., 2017; Milne et al., 2006). This viscosity structure is defined by a lithospheric thickness, an upper mantle viscosity from the base of the lithosphere down to a depth of 671 km, and a lower mantle viscosity from the base of the upper mantle down to a depth of 2886 km. To construct a large ensemble of Earth structure models, we have developed an interpolation algorithm named *ViscoPy* to produce any 1D viscosity structure within a continuous range of values for these three parameters while preserving the location of Preliminary Reference Earth Model discontinuities. We utilise the Earth model parameter ranges used by Bradley et al. (2023) for northwest Europe of 0.1–1×10^{21} Pa s for upper mantle viscosity, 0.1–5×10^{22} Pa s for lower mantle viscosity, and 71–96 km for lithospheric thickness. These values have been selected based on regional published literature for the North Sea region (Shennan et al., 2006, 2018; Bradley et al., 2011, 2009).

2.2.2. Global ice-sheet history

Previous studies have found that ice-sheet history inputs to reconstructions of LIG GIA should include: the Penultimate Glacial Period (ca.194–130 ka) which includes the Penultimate Deglaciation, the primary driver of GIA during the LIG; the Last Glacial Period (ca.100–25 ka), which allows the model output to converge on modern-day topography; and at least two glacial cycles prior to the Penultimate Glacial Period, in order to drive large-scale GIA disequilibrium during the LIG (Dendy et al., 2017). We, therefore, choose to prescribe a global ice-sheet history spanning the last four glacial cycles, from 420 ka to the present day.

We construct our global ice-sheet history to follow the global ice-sheet volume evolution inferred from the δ^{18}O derived global mean

Table 1

Glacial isostatic adjustment model time steps. Description of changes in temporal resolution of ice-sheet history inputs and corresponding RSL outputs to the GIA model.

Age (ka)	Time period	Time step (ka)	Motivation
420–220	Pre-Penultimate Glacial Period	4	Drives long-term GIA signal
220–145	Penultimate Glacial Period	2	PGM 'spin up'
145–142	PGM	1	PGM load
142–126	Penultimate Deglaciation	0.5	Captures deglaciation signal
126–114	LIG	1	High-resolution output for analysis
114–0	Post-LIG	2	Enables convergence iteration

sea-level curve of Waelbroeck et al. (2002), which is provided at a temporal resolution of 1.5 ka. This curve is adopted over newer reconstructions, such as Shakun et al. (2015), as it has a more favourable alignment with the timing of the LIG (130–116 ka). We convert a global mean sea level into a global ice-sheet volume by subtracting it from an estimate of global modern-day (pre-industrial) ice volume (72.1 m SLE), taken from the ICE-6G Last Glacial Period global ice-sheet model (Peltier et al., 2015). In order to remove the impacts of any interglacial ice-sheet melt on our sensitivity results, we restrict the minimum value of global ice-sheet volume to that of the modern-day between 129–116 ka. We employ a linear interpolation procedure based upon the deglaciation portion of ICE-6G to be able to generate global thickness slices of any given total global ice-sheet volume. The deglaciation-only portion is chosen to avoid non-physical ice-mass changes that might occur while interpolating between a glaciating and deglaciating slice of similar volume. For 122 ka to present, we use the global ice-sheet volume curve of ICE-6G (Peltier et al., 2015).

We decrease the temporal resolution of time periods in which detailed ice-geometry changes are less impactful on LIG RSL (Table 1), in order to improve computational efficiency while prescribing higher resolution time steps during the Penultimate deglaciation (0.5 ka) and LIG (1 ka). This allows us to capture shorter time-scale mass changes and to facilitate high temporal-resolution analysis of RSL outputs during the LIG. Since we are using ICE-6G deglaciation geometries to construct ice-sheet histories, our current methodology has the inherent assumption that the distribution of ice across the globe for a given global ice-sheet volume was similar to that of the Last Deglaciation for all glacial periods reconstructed. For periods prior to the Penultimate Glacial Period this assumption is likely inconsequential for the purposes of LIG GIA modelling. However, there were large differences in ice distribution between the EIS and NAIS complexes during the PGM compared to the LGM (Dendy et al., 2017; Batchelor et al., 2019). In the following section, we explain how we modify the ice history during the Penultimate Glacial Period accordingly.

2.2.3. Eurasian and North American ice-sheet histories

Previous work has suggested that the timing and rate of deglaciation of both the North American and Eurasian Last Glacial Period ice sheets may play an important role in controlling northwest Eurasian RSL during the Holocene (Bradley et al., 2023). Thus the Penultimate Deglaciation of North America and Eurasia may have had a key role on LIG RSL in northwest Europe (Dendy et al., 2017). However, this is more challenging to constrain than for the LGM due to the relative sparsity of geological data for Penultimate Deglacial ice-sheet changes compared to the most recent Deglaciation (Rohling et al., 2017). To address this lack of data, we develop an experimental design that tests a wide range of Penultimate Deglaciation scenarios that vary in timing and volume for both the EIS and NAIS. The EIS reconstruction utilises our ICESHEET model outputs (building on Pollard et al. (2023) and detailed in Section 2.1.4) given the geographical focus of the research, whereas the NAIS ice load reconstruction is a result of balancing the global sea level budget within ICE-6G. These are then used as input ice sheet histories for the GIA model (Fig. 4).

Each deglaciation scenario for the two ice sheets is characterised by 6 parameters, 3 for NAIS and 3 for EIS: deglaciation start time

(T_{PGM}^{NAIS}, T_{PGM}^{EIS}), deglaciation end time (T_{LIG}^{NAIS}, T_{LIG}^{EIS}), and PGM volume (V_{PGM}^{NAIS}, V_{PGM}^{EIS}). For each ice sheet, the deglaciation portion of the volume time series between T_{PGM} and T_{LIG} is prescribed as a cosine decay function beginning at V_{PGM} and ending at the LIG (modern-day) configuration. In order for the deglaciation volume curve to smoothly join with the preceding Penultimate Glacial Period curve at T_{PGM}, we make two modifications to the volume curve between 220 ka and T_{PGM}: scale in volume, such that the maximum value matches V_{PGM}; and stretch in time, such that V_{PGM} aligns with T_{PGM}. The NAIS volume curve is converted into an ice-sheet thickness series by interpolating ICE-6G, as described previously, while the EIS volume curve uses a given series of ICESHEET-generated deglaciation geometries for interpolation instead.

2.2.4. Ensemble design

For each global ice-history ensemble member, the Eurasian component of the Penultimate Deglaciation is derived from the corresponding series of EIS geometries, modelled with ICESHEET, as described in Section 2.1.4. Therefore, V_{PGM}^{EIS} is calculated directly from the PGM geometry from this Eurasian ensemble member. For North America, we derive V_{PGM}^{NAIS} by subtracting the volume of all other ice sheets from the total volume at the PGM, V_{PGM}^{T}. The Penultimate Glacial Maximum volumes for Greenland (10.4 m SLE), Antarctica (78.1 m SLE) and others (0.9 m SLE) are taken from the Last Glacial Maximum configuration of ICE-6G. This assumes that these ice sheets did not exceed their Last Glacial Maximum configurations and that all additional Penultimate Glacial Maximum ice sheet volume is distributed between V_{PGM}^{EIS} and V_{PGM}^{NAIS}.

Since the Waelbrock curve has a reported minimum/maximum value range of ±13 m at the PGM, we choose to incorporate this uncertainty by assuming V_{PGM}^{T} can be described as a normal distribution N with a standard deviation σ of 4.3 m, such that 99.7% of the probability density is within 13 m of the mean μ. Instances of V_{PGM}^{NA} are therefore drawn from the distribution,

$$V_{PGM}^{NAIS} \sim N\left(\mu = V_{PGM}^{T} - \left(V_{PGM}^{EIS} + V_{PGM}^{GIS} + V_{PGM}^{AIS} + V_{PGM}^{G}\right), \sigma = 4.3\right),$$

where V_{PGM}^{GIS}, V_{PGM}^{AIS}, and V_{PGM}^{G} represent the PGM ice-sheet volume of the Greenland ice sheet, Antarctic ice sheet, and glaciers, respectively.

We design a 532-member ensemble to match the sample size of the previously generated Eurasian deglaciation series (Fig. 3). We sample over the 10 parameters controlling the PGM ice-sheet deglaciation timing and volume, Eurasian margin asynchrony, and Earth model rheology. The rheological parameters are used to calculate the Love numbers (Peltier, 1974; Kendall et al., 2005) associated with each Earth model structure. One individual parameter combination translates into a single RSL output via our combined model workflow (Fig. 4). Our parameter sample results in 532 ice-sheet history inputs that vary in NAIS and EIS volumes and deglaciation patterns during the Penultimate Glacial Period (Fig. 5).

2.2.5. Sobol sensitivity analysis

We employ Sobol sensitivity analysis (Sobol', 1990) to decompose the ensemble variance at four times throughout the LIG (126, 122, 118 and 116 ka) into per-parameter contributions, to understand the importance of each parameter on the modelled LIG RSL, as well as any large variations in the spatial influence of each parameter (Fig. 6).
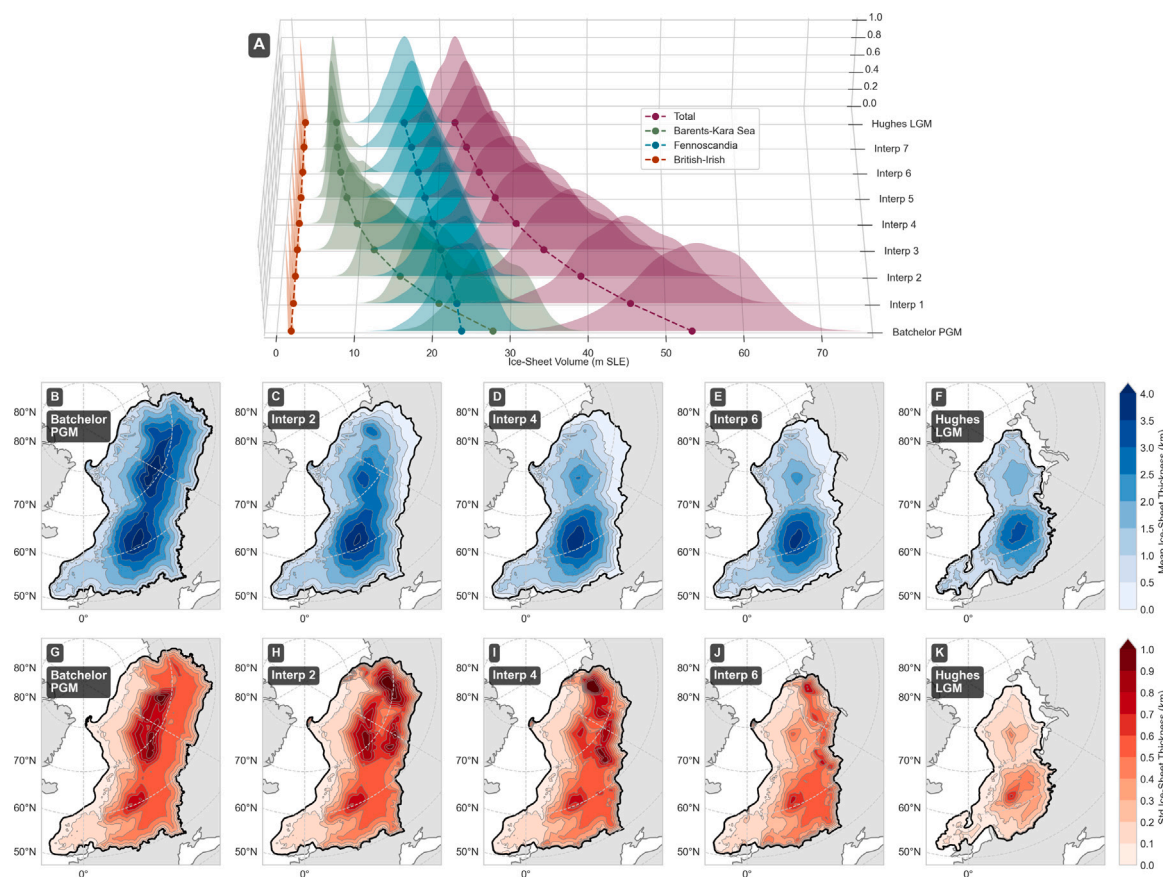
Fig. 3. Eurasian Penultimate Deglaciation Ice-Sheet Ensemble. (A) Distribution of EIS volumes generated by ICESHEET, shown by region, for margins between the PGM Batchelor et al. (2019) and LGM Hughes et al. (2016) configurations (the pattern of deglaciation for ice sheet margins equivalent maximum LGM margin of Hughes, or smaller, is assumed to follow the same pattern as reconstructed for the LGM and therefore not shown here). The mean volume is shown by the dotted line. Mean (B-F) and standard deviation (G-K) of ice-sheet thickness across the ensemble of model outputs is shown for 5 margins within the deglaciation series. The maximum extent across the ensemble for a given time slice is shown by the black contour.

In order to reduce the computational requirements of this analysis, our RSL ensemble is first restricted to northwest Europe, resampled onto a coarser model grid (using a window coarsening of size 6), and model grid cells that do not intersect modern-day ocean or coastline are excluded, leaving 3059 remaining grid cells. To facilitate the evaluation of additional parameter combinations outside of the initial sample, we train independent Gaussian process emulators on the 532 simulated RSL values at each grid cell and time. Rather than using the shear stress input parameters directly, we both train the emulators and perform our sensitivity analysis on calculated regional ice-sheet volume values for the Barents-Kara Sea, Fennoscandian, and British-Irish sections of the PGM EIS for each member of our ensemble. This means that we emulate RSL at each grid cell in our domain as a function of the parameters detailed in Table 2. Each Gaussian process uses a Matern-52 kernel with independent length scales for each input parameter and the inclusion of an infinitesimal nugget term (the emulator hyperparameters are included in the Zenodo data repository). Prediction performance was validated using leave-one-out cross-validation on a small subset of 4 emulators, randomly selected from the spatiotemporal domain, which produced an average root mean squared error of 3.1 m SLE (Figure 12).

We generate a 1024-member Sobol sequence, defining the specific locations within the parameter space at which our emulators are evaluated for input to the Sobol decomposition algorithm. To aid the interpretation of our results, we choose to group parameters into Earth model, ice-sheet volume, and deglaciation timing categories as detailed in Table 2. Our decomposition quantifies three types of parameter contributions to the RSL output variance: first-order effects,

Table 2

Sensitivity and uncertainty metrics. Parameters used for sensitivity and uncertainty analysis.

Name	Symbol	Group
Upper Mantle Viscosity	ν_{UM}	Earth Model
Lower Mantle Viscosity	ν_{LM}	Earth Model
Lithospheric Thickness	L	Earth Model
Barents-Kara Sea Ice Volume	V_{BKS}^{Er}	Ice-Sheet Volume
Fennoscandian Ice Volume	V_{F}^{Er}	Ice-Sheet Volume
British-Irish Ice Volume	V_{BI}^{Er}	Ice-Sheet Volume
NA + Er PGM Volume	V_{PGM}^{NA+Er}	Ice-Sheet Volume
Async Power	A_{θ}	Deglaciation Timing
Async Angle	A_{n}	Deglaciation Timing
Er Deglaciation Start Time	T_{PGM}^{Er}	Deglaciation Timing
Er Deglaciation End Time	T_{LIG}^{Er}	Deglaciation Timing
NA Deglaciation Start Time	T_{PGM}^{NA}	Deglaciation Timing
NA Deglaciation End Time	T_{LIG}^{NA}	Deglaciation Timing

describing the independent contribution of each parameter; second-order effects, resulting from parameter-pair interactions; and total-order effects, representing the summed contribution of all interactions and the independent contributions for each parameter.
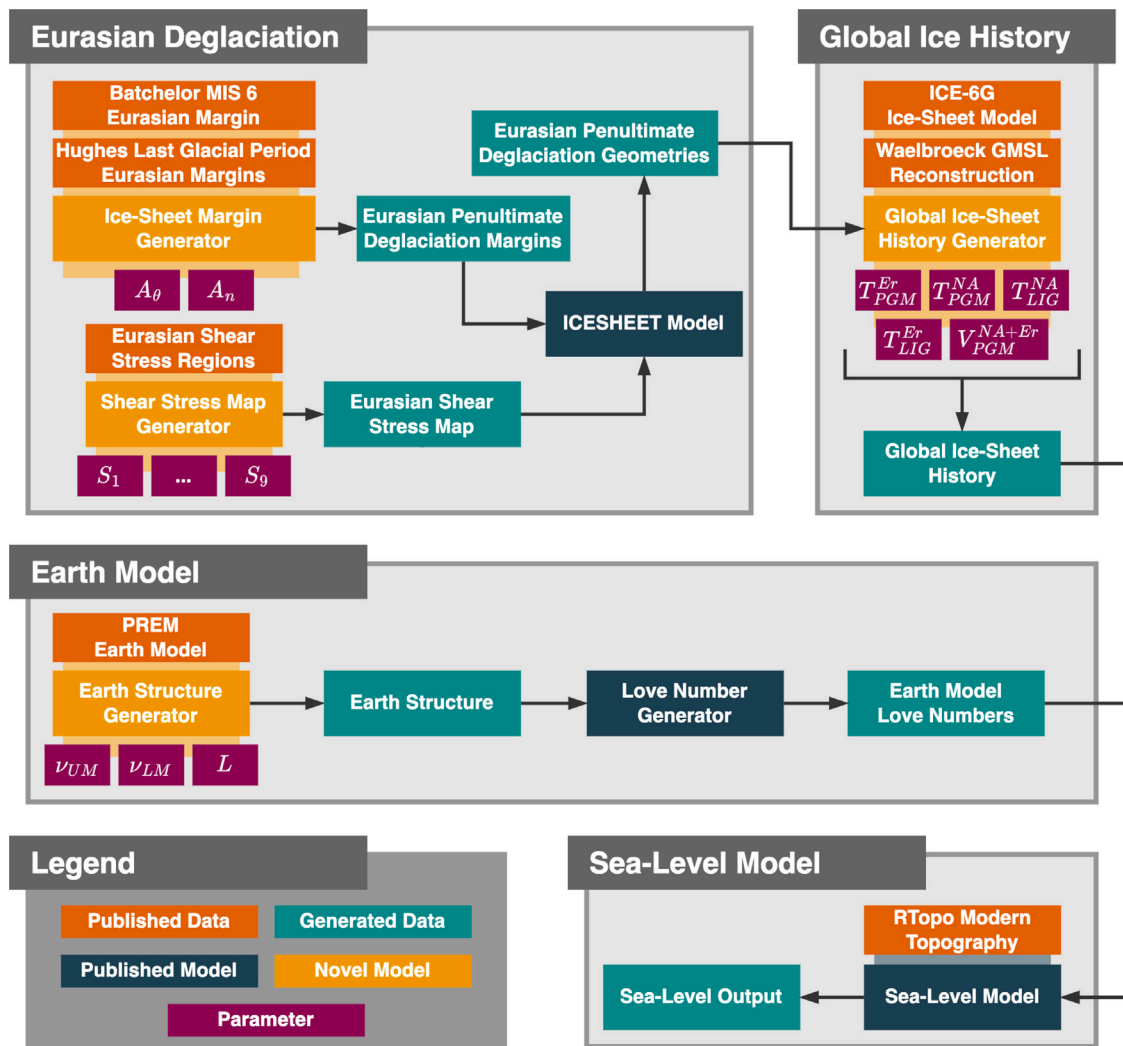
Fig. 4. Sensitivity Ensemble Workflow. Flowchart showing the overall experimental design used in this paper. Key sections of work are grouped together. Numerical models (blue/yellow) are shown with their respective data inputs (orange/green) and parameters (purple). LGP is for the Last Glacial Period. PD refers to the Penultimate Deglaciation. PREM refers to the Preliminary Reference Earth Model.

3. Results

3.1. Last interglacial relative sea level

Our ensemble of 532 LIG simulations show that, on average, GIA drove RSL to remain significantly higher throughout the LIG relative to the present day (pre-industrial) under areas directly covered by the EIS (Fig. 6). This is because the EIS was larger at the PGM than the LGM and therefore depressed the solid Earth more. In the North Sea region, we find LIG RSL was almost exclusively higher than modern by an average of 30 ± 10 m, and in some places over 50 ± 30 m. However, we found that the spatial average rate of RSL change over the full Eurasian region was -2 mm yr^{-1} and was predominantly negative except for in the southern North Sea and Greenland-Iceland-Norwegian (GIN) Sea, where forebulge collapse leads to a maximum rate of change of 1 mm yr^{-1} and 5 mm yr^{-1} respectively.

There is also a high level of uncertainty in our ensemble throughout the Eurasian region, particularly in locations previously covered by the PGP EIS mass. Disequilibrated topography relaxes towards isostatic equilibrium as the interglacial progresses and results in a reduction in the spatially averaged uncertainty in RSL values later in the LIG. The average RSL standard deviation across the North Sea region reduces from ± 21 m at 126 ka to ± 14 m at 116 ka, reducing approximately linearly by ≈ 0.7 m per ka. This uncertainty is highly spatially variable

and we find that the southern North Sea has a relatively low uncertainty throughout the interglacial of $\approx \pm 5$ m, while further north areas covered by the British-Irish ice-sheet experience RSL uncertainties up to an order of magnitude greater.

3.2. Relative sea-level sensitivity

Using our Sobol sensitivity analysis described in the Methods, We find that the Earth model parameters make the largest first-order contribution to LIG RSL uncertainty across the Eurasian region for all times considered (Fig. 7) as well as having the largest magnitude of uncertainty attributed to parameter interaction effects (Figure 10). The influence of the wide range of ice-sheet volumes in our ensemble is high in the Barents-Kara Sea region, contributing greater than 20 m uncertainty under the region previously loaded by the EIS. However, in the Baltic Sea region, which was previously covered by the Fennoscandian portion of the ice sheet, we find that the contribution of ice-sheet mass to the RSL uncertainty significantly reduces from greater than 20 m at 126 ka to less than 3 m by 116 ka. The influence of ice-sheet deglaciation timing on uncertainty is limited to the Siberian coastline and the northern Baltic Sea region at 126 ka (Fig. 7I), reducing to less than 5 m by 116 ka (Fig. 7L).

There is significant variation in the magnitude and spatial scope of the first-order influence of individual Earth model parameters. We
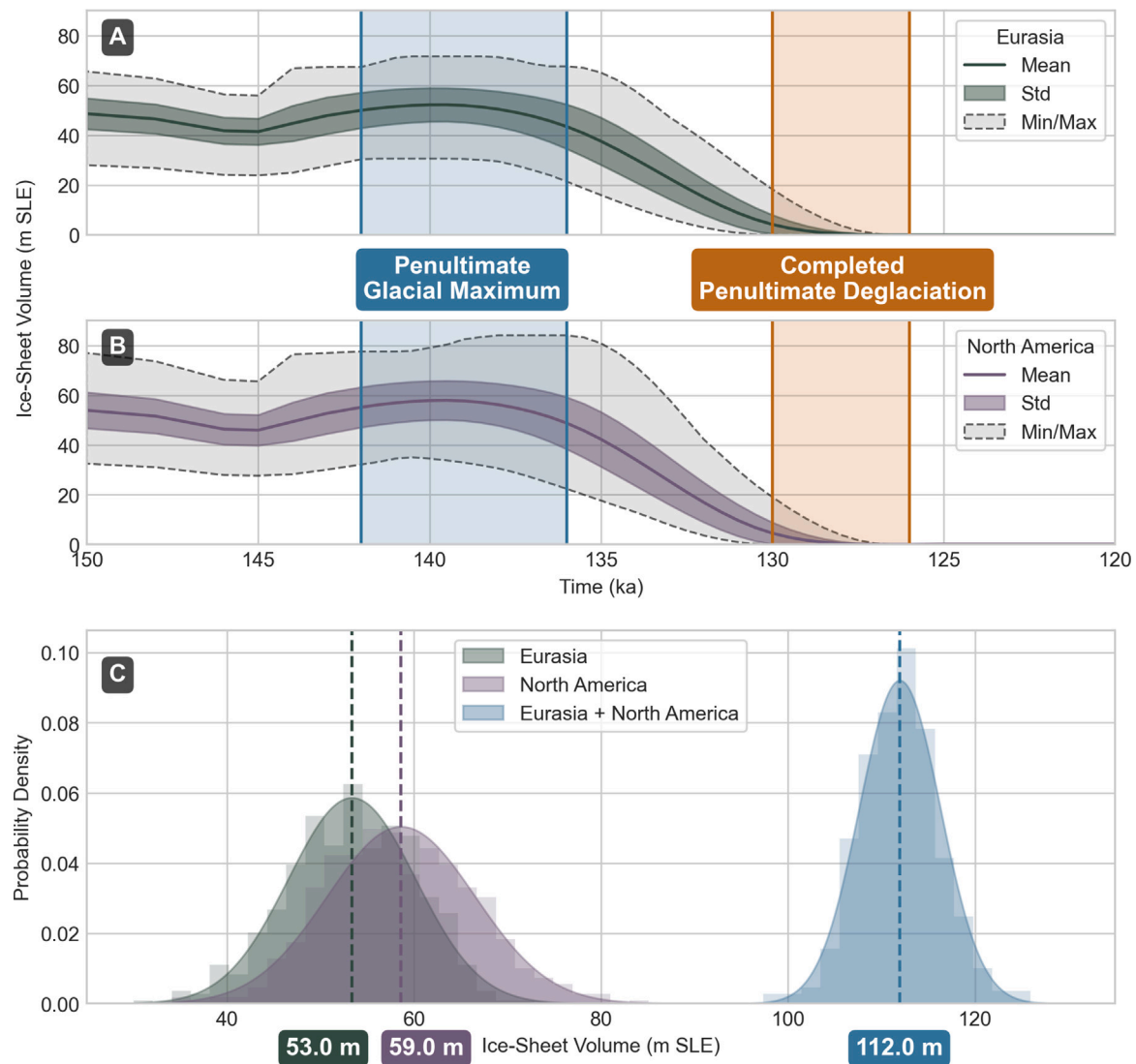
Fig. 5. Distributions of Global Ice-Sheet Input Parameters. (A) Mean (solid line), standard deviation (shaded coloured region), and maximum/minimum values (grey dotted lines) of the ensemble of ice-sheet volume timeseries, shown between 150 and 120 ka, tested for the EIS. (B) Same as (A) but for the NAIS. (C) The probability density function of normal distributions fitted to the sample of PGM ice-sheet volumes for the EIS (derived from the ICESHEET model ensemble), total EIS and NAIS (defined from uncertainty in the Waelbroeck et al. (2002) δ^{18}O curve), and NAIS (resulting from the residual).

find that the upper mantle viscosity is a dominant source of uncertainty in a number of regions: the central North Sea, GIN Sea, Barents Sea, and northern Kara Sea, Baltic Sea, and Siberian coastline regions (see locations in Fig. 1). The lower mantle viscosity RSL uncertainty contribution is concentrated around the northern Baltic Sea, where it contributes greater than 20 m, and the Fennoscandian coastline. In contrast, we find that the lithospheric thickness makes a relatively minimal contribution and, of all regions considered, is most influential in the GIN Sea, where the total-order contribution still only equates to 15% of the overall average RSL uncertainty (Fig. 6G).

Parameter interaction effects (*i.e.*, differences in the magnitude of RSL variance that results from changing multiple parameters simultaneously when compared against the RSL variance that results from changing parameters individually) are most influential in the Baltic Sea, Barents-Kara Sea and GIN Seas (Figure 11). The upper and lower mantle viscosities are most interactive in all regions, but we find that there is a strong interaction between the volume of the Barents-Kara Sea ice mass and the other ice-sheet regions, perhaps due to a larger Barents-Kara Sea ice volume co-existing with relatively large ice-sheet volumes from other regions. The viscosity parameters are responsible for producing the most extreme ensemble members (quantified by the

average standard deviation from the ensemble mean) for most regions. However, the Barents-Kara Sea is more influenced by the volume of the Fennoscandian and Barents-Kara Sea ice sheets than viscosity.

3.3. Rate of relative sea-level change sensitivity

The rate of RSL change may be important to consider when attempting to fingerprint interglacial ice-sheet melt. Therefore, in addition to the magnitude of RSL at individual times throughout the LIG, we performed the sensitivity analysis on the average rate of RSL change across the LIG (Fig. 9). The Barents-Kara, Norwegian and Baltic Seas have the highest uncertainty in regards to the modelled rate of RSL change, reaching 4 mm yr^{-1} uncertainty in some places (Fig. 9). The relative contributions of each parameter to the uncertainty in RSL rate of change are of similar magnitude to those previously discussed for the RSL uncertainty. However, differences between the rate of change and RSL exist in the North Sea region, where the rate is far less uncertain. We find that the Earth model contribution to uncertainty in rate of RSL change substantially decreases in the Barents-Kara and Baltic Sea regions, while the ice-sheet volume influence remains concentrated around the Barents-Kara Sea.
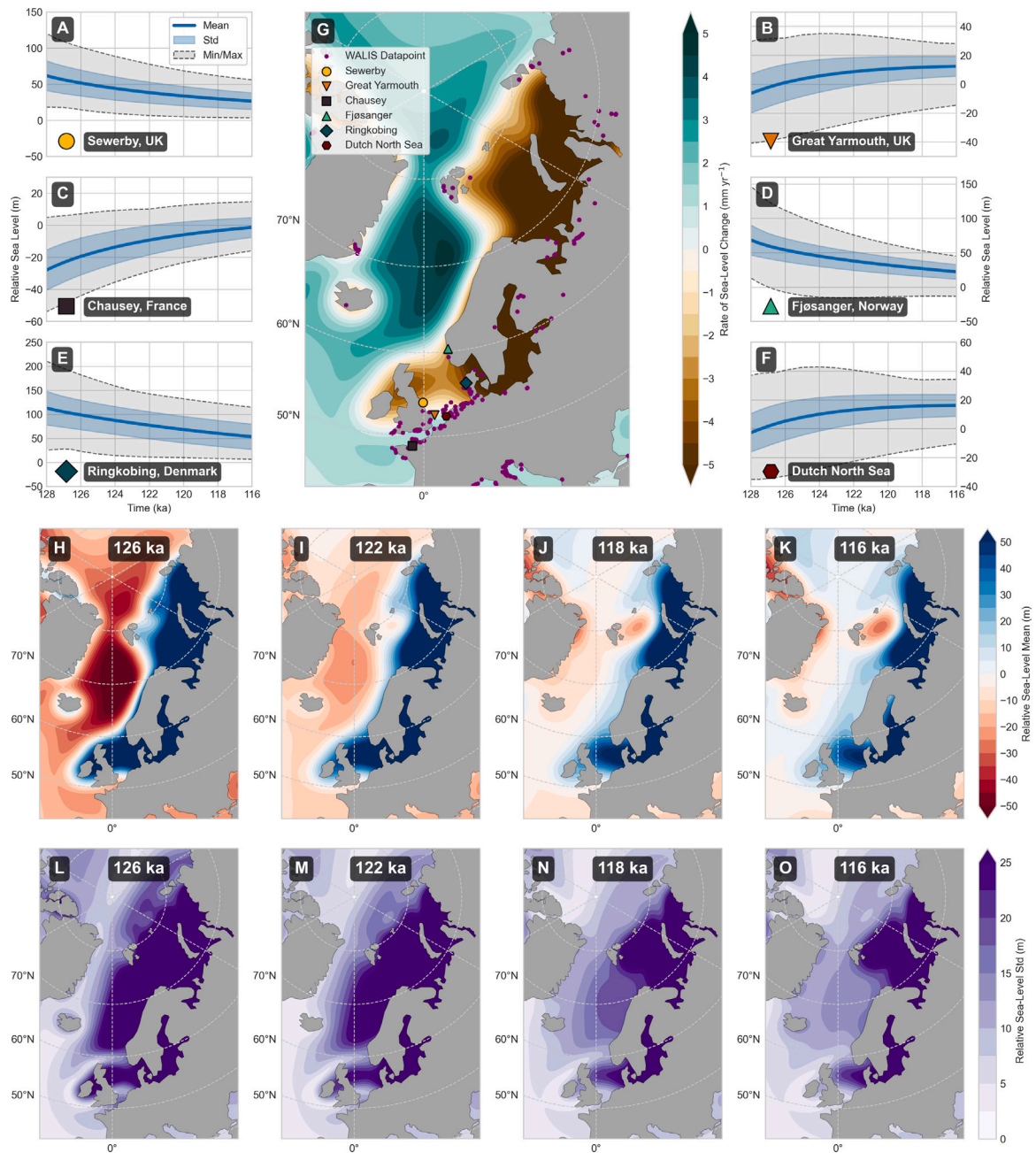
Fig. 6. Last Interglacial Relative Sea-Level Ensemble. (A-F) Mean (solid line), standard deviation (shaded blue region) and minimum/maximum (grey dotted lines) values of the RSL ensemble, relative to the present day, shown for six selected locations that reflect the transects of RSL data shown Cohen et al. (2022). (G) Ensemble mean rate of Eurasian LIG RSL change. Purple points show locations of empirical RSL data from the WALIS database (Rovere et al., 2023). The marker for location (A-F) is also plotted on this map. (H-K) Ensemble mean RSL shown for four times (126, 122, 118 and 116 ka), relative to the present day. (L-O) Same as (H-K), but showing the RSL standard deviation across the ensemble.

4. Discussion

We have systematically tested, for the first time, a suite of LIG RSL scenarios that vary in the configuration, volume, and timing of the Penultimate Deglaciation of the NAIS and EIS; as well as in the upper and lower mantle viscosities and lithospheric thickness of a radially varying solid Earth model. We found that RSL changes across northwest Eurasia during the LIG had a pattern different to that in the current interglacial (Bradley et al., 2023), due to the strong influence of GIA from ice-sheet changes during the Penultimate Deglaciation of the Eurasian ice sheet, which differed to that during the Last Glacial Batchelor et al. (2019). Areas that were directly beneath the former PGM EIS experienced high RSL values, in some places exceeding 50 m, such as

in the Baltic Sea, central North Sea, and Barents-Kara Sea. In contrast, the GIN Sea and areas of the North Atlantic Ocean had lower RSL, likely due to the combined influence of forebulge formation and ice-mass-driven perturbations of the Earth's rotational axis. We found that the magnitude of RSL decreases in many regions and the region of forebulge subsidence migrates landwards towards the ice load centre as the system approaches isostatic equilibrium during the LIG (Fig. 6). By 116 ka, the previously low RSL values in the GIN Sea and North Atlantic Ocean had relaxed to near modern levels, while the RSL values in the Baltic Sea, Barents Sea, southern Kara Sea, and central North Sea had also relaxed but remained significantly different from modern.

Our ensemble resulted in high levels of uncertainty in GIA-induced RSL changes during the LIG, with an average of 34 m uncertainty
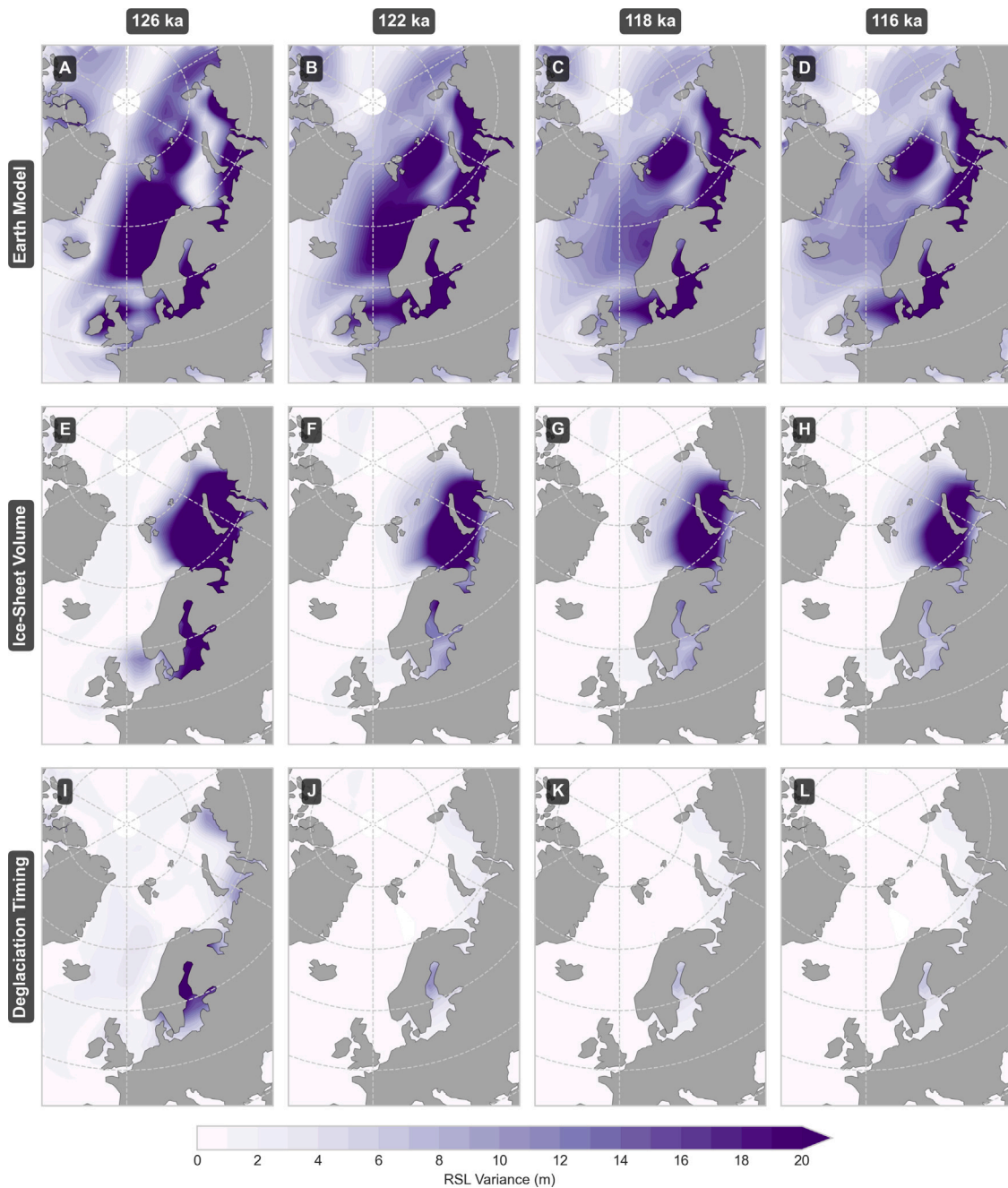
Fig. 7. Relative Sea-Level Sensitivity: Grouped Parameters. Decomposition of the RSL ensemble uncertainty at 126, 122, 118 and 116 ka. RSL uncertainty is shown as the summed 1st-order sensitivities for three groups of model parameters: (A-D) Earth model, (E-H) Eurasian PGM ice-sheet volume, and (I-L) Penultimate Deglaciation timing parameters.

over all regions at 126 ka, reducing to an average of 21 m by 116 ka. However, there is variability in the level of uncertainty between regions with the English Channel, GIN Sea, and North Sea having the lowest uncertainty (averaging 12 m, 16 m and 21 m respectively at 126 ka) while the Barents-Kara and Baltic Seas are highly uncertain (averaging 50 m and 72 m at 126 ka respectively). Parameter-wise sensitivity decomposition shows that, for almost all times and regions considered, uncertainty in the Earth model parameters dominate the RSL sensitivity and that, in particular, the upper mantle viscosity is the most important quantity in determining regional RSL. It is only in areas towards the centre of large ice-mass loading, such as the Barents-Kara Sea and areas of the Baltic Sea, that the regional volumes of the EIS become more important than Earth model parameters in determining RSL. We find that the timing of the NAIS deglaciation plays a negligible role in determining RSL in all regions, while the timing of the Eurasian

deglaciation plays a moderate role in the Baltic Sea towards the start of the LIG. The work by Dendy et al. (2017) had previously demonstrated that Eurasian ice-sheet geometry uncertainty is a major contributor to uncertainty in records of RSL close to the former ice sheet and, while our work agrees with these results, we find that the influence of ice-sheet geometry uncertainty is more spatially limited to locations directly underneath former ice-sheet loads when compared against Earth model uncertainty, particularly upper mantle viscosity (Fig. 8). These differing conclusions can likely be explained by Dendy et al. (2017)'s focus on Earth model uncertainty in the far-field locations of Bermuda and the Seychelles, combined with their one-at-a-time experimental design making it difficult to quantify relative parameter importance to near-field RSL. Therefore, in contrast to the Dutton et al. (2015) suggestions that constraining near-field ice-sheet extent and climate are key, our work suggests that constraining Earth model uncertainty is of
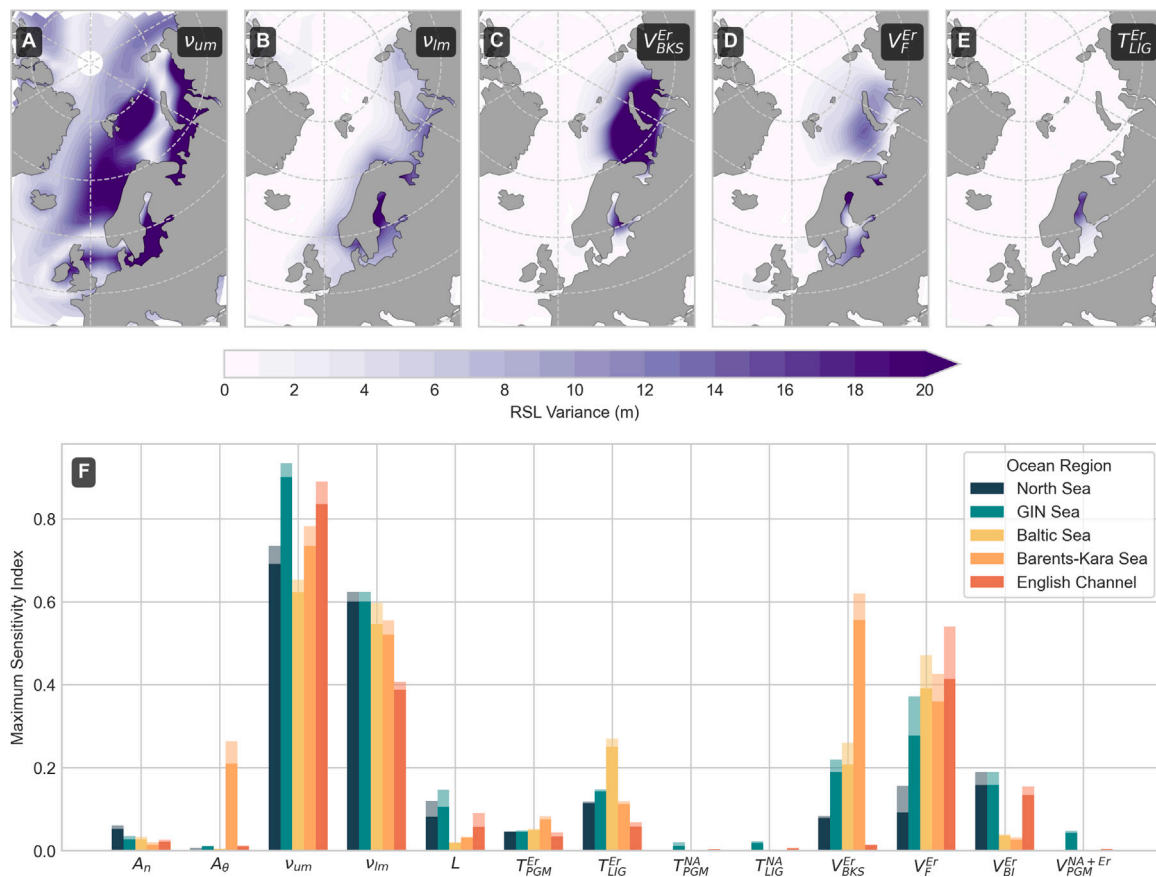
Fig. 8. Relative Sea-Level Sensitivity: Individual Parameters. (A-E) Sensitivity decomposition of RSL uncertainty, averaged over the LIG, from the 5 most influential parameters (Table 2). (F) Maximum 1st-order sensitivity index for each parameter with respect to the time-averaged RSL variance in 5 different marine regions (where RSL will be recorded at the coastline), with the total order contribution shown as the lighter coloured bar.

greatest importance for enabling the use of near-field RSL records in the reconstruction of LIG RSL changes.

In order to limit the size of our ensemble parameter space, we have made several simplifying assumptions when considering the broad range of sources of uncertainty that may contribute to uncertainty in LIG RSL. We adopt the approach of similar studies by assuming a simple, 1D, globally uniform Earth structure for determining the solid Earth response to ice-sheet loading (Bradley et al., 2023; Dendy et al., 2017). Therefore, we cannot account for potential lateral variability in mantle viscosity and lithospheric thickness over our study area that would be captured through the use of 3D Earth models. While the computational cost was infeasible within our ensemble design, we recommend the influence of 3D Earth models on LIG RSL variability be tested in future work. However, as van der Wal et al. (2013) highlight, there are also inherent uncertainties in the flow laws and Earth materials in 3D Earth models, which would need to be assessed as part of future sensitivity studies.

Future work to reduce the uncertainties in LIG RSL must be underpinned by empirical data. Our suggests that data records subject to the lowest GIA uncertainty are those located in the southern North Sea, the English Channel and GIN Sea regions (Fig. 6), and those record which date towards the end of the LIG. We therefore recommend that future RSL data collection focus on these regions and time periods in order to minimise the influence of GIA uncertainty on the interpretation of records. Records collected in the Baltic Sea, central North Sea, and southern Barents-Kara Sea of any LIG age should pay particular attention to characterising Earth model uncertainty, while data points in the Baltic Sea and Barents-Kara Sea are also subject to uncertainty from the corresponding regional volume of the EIS. We find that the timing of the Eurasian deglaciation plays a minor role, except for RSL

data constrained to the beginning of the LIG. We find that the NAIS complex plays a negligible role in determining the overall uncertainty of northwest Eurasian RSL during the LIG, in contrast to the Last Deglaciation (Bradley et al., 2023), but that this sensitivity is likely to change if later deglaciation timings are considered.

Our ensemble of EIS simulations was generated assuming a single maximum ice-sheet extent for all ensemble members but previous work by Pollard et al. (2023) has suggested that including a variable PGM ice extent may have contributed up to an additional 10% variability in the Eurasian PGM ice-sheet volume. Varying PGM margins in our ensemble would have added significant complexity to the interpretation of asynchrony parameter sensitivity and would likely have made a minor contribution to the overall uncertainty. We similarly do not explore the uncertainty of differing GIA models, but as Simon and Riva (2020) identify a resulting RSL uncertainty of ~ 0.6–0.8 mm yr^{-1} for the North Sea due to GIA model uncertainty, this is considered negligible compared to the total uncertainty in LIG RSL due to ice sheet and Earth model parameters.

In generating global ice-sheet histories, we chose to use δ^{18}O as a proxy for total global ice-sheet volume due to the absence of alternative ice-volume datasets. There are multiple sources of uncertainty in using δ^{18}O data as a proxy for global ice-sheet volume including: interpreting a global complication of δ^{18}O while accounting for spatiotemporal variability due to patterns of climate and ocean circulation that affect isotopic fractionation; temporal uncertainty from dating records from which δ^{18}O values have been derived; and calibrating the relationship between proxy values and the true δ^{18}O value, including the influence of local effects, such as local ocean temperature, on these relationships (Shakun et al., 2015; Waelbroeck et al., 2002). While it was not within the scope of this study, the use of alternative global ice volume
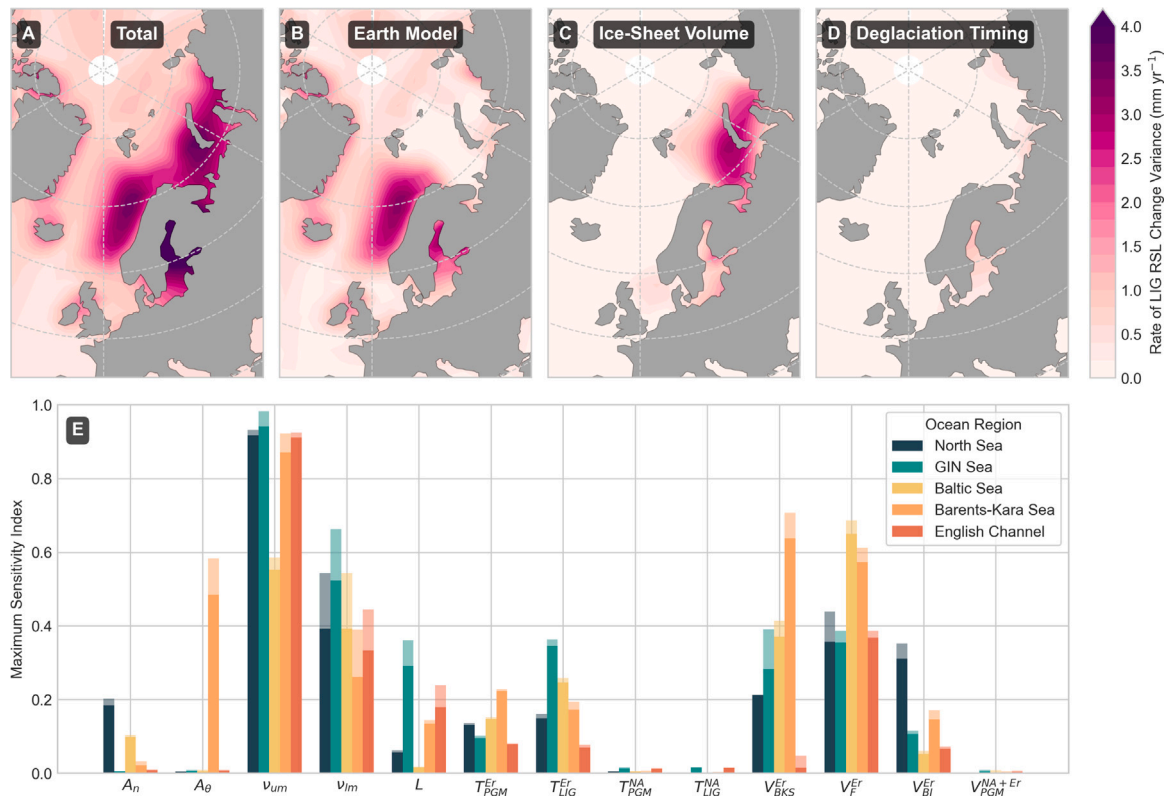
Fig. 9. Rate of Relative Sea-Level Change Sensitivity: Grouped Parameters. (A-D) Decomposition of the rate of LIG RSL change variance into parameter groups. (E). Maximum percentage 1st order parameter contribution to the RSL rate of change variance in 5 different ocean regions, with the total order contribution shown as the lighter coloured bar.

reconstructions in our work may have resulted in a wider range of possible timing and magnitude changes in global ice-sheet volume and thus altered the range of possible RSL outputs. However, we did take account of the uncertainty in our δ^{18}O derived global ice-sheet volume by representing the inferred combined NAIS and EIS PGM volume as a normally distributed parameter reflecting the δ^{18}O uncertainty assessment of Waelbroeck et al. (2002). This only had a negligible contribution to uncertainty in LIG RSL in all regions considered.

The overall pattern of mean and variance in LIG RSL is similar to the suite of GIA scenarios tested by Barnett et al. (2023), which encompassed changes in EIS volume and Earth model configuration, but our study suggests three key differences: more extensive subsidence surrounding the British Isle due to a slightly thicker ice load over the British Isles and North Sea in our experiments, a greater RSL uncertainty in the GIN Sea at the beginning of the LIG, and more substantial subsidence in the Baltic and North Sea regions by the end of the LIG. We find a similar pattern of uncertainty in the North Sea region to Barnett et al. (2023), likely due to the presence of an ice bridge connecting the British-Irish and Fennoscandian ice sheets, similar to that which occurred during the LGM (Gandy et al., 2021). The sensitivity experiments performed by Dendy et al. (2017) implicitly concluded that Eurasian RSL at the end of the LIG was highly dependent on the volume of the EIS at the PGM, generating absolute RSL differences of greater than 6 m in most regions when comparing the effect of the larger Lambeck et al. (2006) EIS PGM geometry against the smaller LGM ICE-6G geometry (Peltier et al., 2015). While we did not test Eurasian volumes as small as in ICE-6G (23.5 m SLE), we attributed a similar magnitude of North Sea RSL variance to EIS volume uncertainty to that calculated by Dendy et al. (2017) (2–4 m) as well as observing similarly large variances in regions beneath the former ice-sheet load. Dendy et al. (2017) also suggested that, beyond the former ice margin, the influence of ice-mass changes on the perturbation of the Earth's rotational axis acted to reduce RSL for larger ice sheets by greater than 6 m for an invariant Earth model. While we do not

explicitly isolate the contribution of rotational effects in this work, these effects are included in our GIA modelling. We can expect the changes in RSL driven by rotational perturbations to be small compared to the influence of solid Earth deformation in the near-field northwest Eurasian region.

Utilising LIG RSL data from near-field locations for the purpose of developing LIG fingerprints of ice sheet melt is a major goal for the palaeo sea-level community (Dutton et al., 2015; Hay et al., 2014). Importantly, our work suggests that quantifying the influence of and uncertainty in ongoing GIA driven by the preceding deglaciation is essential to unearthing these sea-level fingerprints, and identifies regions where fingerprinting and data collection efforts may be most fruitful. Large uncertainty on the GIA signal may hamper efforts to use data from the Barents-Kara and Baltic Seas, while data acquired in southwestern Eurasian regions where overall RSL uncertainty is lowest, such as the English Channel, may provide more insight on LIG ice melt sources, and importantly the rate and magnitudes of ice sheet melt in response to polar warming.

5. Conclusions

Quantifying the contribution and uncertainty of GIA to LIG RSL remains a challenge due to the significant uncertainties in past ice-sheet changes and the response of the solid Earth, hampering research that attempts to utilise LIG sea-level record for fingerprinting LIG ice-sheet melt. To address this, we developed an uncertainty quantification framework combining ice-sheet, Earth, and GIA models that is able to systematically assess the uncertainty from two major sources: the volume, configuration, and timing of the Penultimate Deglaciation of the EIS and NAIS; and the 1D model of the viscoelastic solid Earth structure. Utilising our carefully designed ensemble of simulations and advanced statistical techniques, we explored the magnitude and spatial distribution of RSL uncertainty throughout the LIG and attribute the relative contribution of each input parameter to this uncertainty.

We found that the Earth model parameters have the widest spatial influence on uncertainty of both RSL and rate of RSL change, but that the Barents-Kara Sea stands out as being most influenced by the EIS volume. We find that the timing of the ice-sheet deglaciation is most influential on LIG RSL at the beginning of the interglacial and that this influence is concentrated around the Baltic Sea. Parameters controlling the timing and volume of the NAIS play little part in controlling the rate of RSL uncertainty, and the asynchrony of the EIS deglaciation only influences small parts of the Kara Sea. To conclude, our findings suggest that the southern North Sea and the English Channel are regions most suitable for future data collection studies, as they are least affected by GIA uncertainty. We suggest that future work is focused on reducing uncertainty in the Earth model parameters, as they are most influential in quantifying LIG GIA in all regions except those directly under the former EIS. Finally, we highlight the importance of incorporating well-quantified GIA uncertainty in data-driven studies of LIG RSL, particularly for those aimed at quantifying RSL and ice-sheet melt fingerprints.

CRediT authorship contribution statement

Oliver G. Pollard: Designed the experiments (alongside NLMB, LJG and NG), Ran the model simulations, Performed the analysis, Produced the figures, and the manuscript with contributions from all authors. **Natasha L.M. Barlow:** Acquired the funding, Was the source of the idea behind the work, Supervised the work throughout, Advised on the Penultimate Deglaciation experimental design, Contributed to the interpretation and presentation of the work. **Lauren J. Gregoire:** Co-supervised the work, Provided advice and expertise on the experimental design, uncertainty quantification and ice sheet evolution, Contributed to the interpretation and presentation of the work. **Natalya Gomez:** Provided advice and expertise on the experimental design, Glacial isostatic adjustment modelling, Contributed to the ideas behind required Python tools, Contributed to the interpretation and presentation of the work.

Declaration of competing interest

The authors declare that they have no known competing financial interests or personal relationships that could have appeared to influence the work reported in this paper.

Data availability

The data and code associated with this paper are openly available from Zenodo, https://doi.org/10.5281/zenodo.10687144 (Pollard, 2024).

Appendix A. Supplementary data

Supplementary material related to this article can be found online at https://doi.org/10.1016/j.quascirev.2024.108908.

References

Barnett, R.L., Austermann, J., Dyer, B., Telfer, M.W., Barlow, N.L.M., Boulton, S.J., Carr, A.S., Creel, R.C., 2023. Constraining the contribution of the Antarctic Ice Sheet to last interglacial sea level. Sci. Adv. 9 (27), eadf0198. http://dx.doi.org/10.1126/sciadv.adf0198.

Batchelor, C.L., Margold, M., Krapp, M., Murton, D.K., Dalton, A.S., Gibbard, P.L., Stokes, C.R., Murton, J.B., Manica, A., 2019. The configuration of Northern Hemisphere ice sheets through the Quaternary. Nature Commun. 10 (1), 3713. http://dx.doi.org/10.1038/s41467-019-11601-2.

Bradley, S.L., Ely, J.C., Clark, C.D., Edwards, R.J., Shennan, I., 2023. Reconstruction of the palaeo-sea level of Britain and Ireland arising from empirical constraints of ice extent: Implications for regional sea level forecasts and North American ice sheet volume. J. Quat. Sci. jqs.3523. http://dx.doi.org/10.1002/jqs.3523.

Bradley, S.L., Milne, G.A., Shennan, I., Edwards, R., 2011. An improved glacial isostatic adjustment model for the British Isles: Glacial isostatic adjustment model for the British Isles. J. Quat. Sci. 26 (5), 541–552. http://dx.doi.org/10.1002/jqs.1481.

Bradley, S.L., Milne, G.A., Teferle, F.N., Bingley, R.M., Orliac, E.J., 2009. Glacial isostatic adjustment of the British Isles: New constraints from GPS measurements of crustal motion. Geophys. J. Int. 178 (1), 14–22. http://dx.doi.org/10.1111/j.1365-246X.2008.04033.x.

Capron, E., Govin, A., Stone, E.J., Masson-Delmotte, V., Mulitza, S., Otto-Bliesner, B., Rasmussen, T.L., Sime, L.C., Waelbroeck, C., Wolff, E.W., 2014. Temporal and spatial structure of multi-millennial temperature changes at high latitudes during the Last Interglacial. Quat. Sci. Rev. 103, 116–133. http://dx.doi.org/10.1016/j.quascirev.2014.08.018.

Clark, J.A., Lingle, C.S., 1977. Future sea-level changes due to West Antarctic ice sheet fluctuations. Nature 269 (5625), 206–209. http://dx.doi.org/10.1038/269206a0.

Cohen, K.M., Cartelle, V., Barnett, R., Busschers, F.S., Barlow, N.L.M., 2022. Last Interglacial sea-level data points from Northwest Europe. Earth Syst. Sci. Data 14 (6), 2895–2937. http://dx.doi.org/10.5194/essd-14-2895-2022.

Colleoni, F., Wekerle, C., Näslund, J.-O., Brandefelt, J., Masina, S., 2016. Constraint on the penultimate glacial maximum Northern Hemisphere ice topography ($\approx$140 Kyrs BP). Quat. Sci. Rev. 137, 97–112. http://dx.doi.org/10.1016/j.quascirev.2016.01.024.

Coulon, V., Bulthuis, K., Whitehouse, P.L., Sun, S., Haubner, K., Zipf, L., Pattyn, F., 2021. Contrasting response of West and East Antarctic Ice Sheets to Glacial Isostatic Adjustment. J. Geophys. Res. 126 (7), e2020JF006003. http://dx.doi.org/10.1029/2020JF006003.

Dendy, S., Austermann, J., Creveling, J., Mitrovica, J., 2017. Sensitivity of Last Interglacial sea-level high stands to ice sheet configuration during Marine Isotope Stage 6. Quat. Sci. Rev. 171, 234–244. http://dx.doi.org/10.1016/j.quascirev.2017.06.013.

Dutton, A., Carlson, A.E., Long, A.J., Milne, G.A., Clark, P.U., DeConto, R., Horton, B.P., Rahmstorf, S., Raymo, M.E., 2015. Sea-level rise due to polar ice-sheet mass loss during past warm periods. Science 349 (6244), aaa4019. http://dx.doi.org/10.1126/science.aaa4019.

Dyer, B., Austermann, J., D'Andrea, W.J., Creel, R.C., Sandstrom, M.R., Cashman, M., Rovere, A., Raymo, M.E., 2021. Sea-level trends across The Bahamas constrain peak last interglacial ice melt. Proc. Natl. Acad. Sci. 118 (33), e2026839118. http://dx.doi.org/10.1073/pnas.2026839118.

Dziewonski, A.M., Anderson, D.L., 1981. Preliminary reference Earth model. Phys. Earth Planet. Inter. 25 (4), 297–356. http://dx.doi.org/10.1016/0031-9201(81)90046-7.

Ehlers, J., Gibbard, P.L., 2004. Quaternary Glaciations - Extent and Chronology: Part I: Europe. Elsevier.

Ehlers, J., Grube, A., Stephan, H.-J., Wansa, S., 2011. Chapter 13 - Pleistocene Glaciations of North Germany—New Results. In: Ehlers, J., Gibbard, P.L., Hughes, P.D. (Eds.), Developments in Quaternary Sciences. In: Quaternary Glaciations - Extent and Chronology, vol. 15, Elsevier, pp. 149–162. http://dx.doi.org/10.1016/B978-0-444-53447-7.00013-1.

Farrell, W.E., Clark, J.A., 1976. On postglacial sea level. Geophys. J. R. Astron. Soc. 46 (3), 647–667. http://dx.doi.org/10.1111/j.1365-246X.1976.tb01252.x.

Gandy, N., Gregoire, L.J., Ely, J.C., Cornford, S.L., Clark, C.D., Hodgson, D.M., 2021. Collapse of the last Eurasian ice sheet in the North Sea modulated by combined processes of ice flow, surface melt, and marine ice sheet instabilities. J. Geophys. Res. 126 (4), http://dx.doi.org/10.1029/2020JF005755.

Gowan, E.J., Tregoning, P., Purcell, A., Lea, J., Fransner, O.J., Noormets, R., Dowdeswell, J.A., 2016. ICESHEET 1.0: A program to produce paleo-ice sheet reconstructions with minimal assumptions. Geosci. Model Dev. 9 (5), 1673–1682. http://dx.doi.org/10.5194/gmd-9-1673-2016.

Gowan, E.J., Zhang, X., Khosravi, S., Rovere, A., Stocchi, P., Hughes, A.L.C., Gyllencreutz, R., Mangerud, J., Svendsen, J.-I., Lohmann, G., 2021. A new global ice sheet reconstruction for the past 80 000 years. Nature Commun. 12 (1), 1199. http://dx.doi.org/10.1038/s41467-021-21469-w.

Hay, C., Mitrovica, J.X., Gomez, N., Creveling, J.R., Austermann, J., E. Kopp, R., 2014. The sea-level fingerprints of ice-sheet collapse during interglacial periods. Quat. Sci. Rev. 87, 60–69. http://dx.doi.org/10.1016/j.quascirev.2013.12.022.

Hughes, A.L.C., Gyllencreutz, R., Lohne, Ø.S., Mangerud, J., Svendsen, J.I., 2016. The last Eurasian ice sheets – a chronological database and time-slice reconstruction, DATED-1. Boreas 45 (1), 1–45. http://dx.doi.org/10.1111/bor.12142.

IPCC, 2022. The Ocean and Cryosphere in a Changing Climate: Special Report of the Intergovernmental Panel on Climate Change. Cambridge University Press, Cambridge, http://dx.doi.org/10.1017/9781009157964.

Kendall, R.A., Mitrovica, J.X., Milne, G.A., 2005. On post-glacial sea level - II. Numerical formulation and comparative results on spherically symmetric models. Geophys. J. Int. 161 (3), 679–706. http://dx.doi.org/10.1111/j.1365-246X.2005.02553.x.

Kopp, R.E., DeConto, R.M., Bader, D.A., Hay, C.C., Horton, R.M., Kulp, S., Oppenheimer, M., Pollard, D., Strauss, B.H., 2017. Evolving understanding of Antarctic ice-sheet physics and ambiguity in probabilistic sea-level projections. Earth's Future 5 (12), 1217–1233. http://dx.doi.org/10.1002/2017EF000663.

Lambeck, K., Purcell, A., Dutton, A., 2012. The anatomy of interglacial sea levels: The relationship between sea levels and ice volumes during the last interglacial. Earth Planet. Sci. Lett. 315–316, 4–11. http://dx.doi.org/10.1016/j.epsl.2011.08.026.

Lambeck, K., Purcell, A., Funder, S., KJaeR, K.H., Larsen, E., Moller, P., 2006. Constraints on the Late Saalian to early Middle Weichselian ice sheet of Eurasia from field data and rebound modelling. Boreas 35 (3), 539–575. http://dx.doi.org/10.1080/03009480600781875.

Lambeck, K., Rouby, H., Purcell, A., Sun, Y., Sambridge, M., 2014. Sea level and global ice volumes from the last glacial maximum to the Holocene. Proc. Natl. Acad. Sci. 111 (43), 15296–15303. http://dx.doi.org/10.1073/pnas.1411762111.

Lin, Y., Hibbert, F.D., Whitehouse, P.L., Woodroffe, S.A., Purcell, A., Shennan, I., Bradley, S.L., 2021. A reconciled solution of Meltwater Pulse 1A sources using sea-level fingerprinting. Nature Commun. 12 (1), 2015. http://dx.doi.org/10.1038/s41467-021-21990-y.

Long, A.J., Barlow, N.L.M., Busschers, F.S., Cohen, K.M., Gehrels, W.R., Wake, L.M., 2015. Near-field sea-level variability in Northwest Europe and ice sheet stability during the last interglacial. Quat. Sci. Rev. 126, 26–40. http://dx.doi.org/10.1016/j.quascirev.2015.08.021.

Milne, G., Shennan, I., Youngs, B., Waugh, A., Teferle, F., Bingley, R., Bassett, S., Cuthbert-Brown, C., Bradley, S., 2006. Modelling the glacial isostatic adjustment of the UK region. Phil. Trans. R. Soc. A 364 (1841), 931–948. http://dx.doi.org/10.1098/rsta.2006.1747.

Mitrovica, J.X., Gomez, N., Morrow, E., Hay, C., Latychev, K., Tamisiea, M.E., 2011. On the robustness of predictions of sea level fingerprints. Geophys. J. Int. 187 (2), 729–742. http://dx.doi.org/10.1111/j.1365-246X.2011.05090.x.

Mitrovica, J.X., Milne, G.A., Davis, J.L., 2001. Glacial isostatic adjustment on a rotating Earth. Geophys. J. Int. 147 (3), 562–578. http://dx.doi.org/10.1046/j.1365-246x.2001.01550.x.

O'Leary, M.J., Hearty, P.J., Thompson, W.G., Raymo, M.E., Mitrovica, J.X., Webster, J.M., 2013. Ice sheet collapse following a prolonged period of stable sea level during the last interglacial. Nat. Geosci. 6 (9), 796–800. http://dx.doi.org/10.1038/ngeo1890.

Otto-Bliesner, B.L., Marshall, S.J., Overpeck, J.T., Miller, G.H., Hu, A., CAPE Last Interglacial Project members, 2006. Simulating Arctic climate warmth and icefield retreat in the last interglaciation. Science 311 (5768), 1751–1753. http://dx.doi.org/10.1126/science.1120808.

Patton, H., Hubbard, A., Andreassen, K., Auriac, A., Whitehouse, P.L., Stroeven, A.P., Shackleton, C., Winsborrow, M., Heyman, J., Hall, A.M., 2017. Deglaciation of the Eurasian ice sheet complex. Quat. Sci. Rev. 169, 148–172. http://dx.doi.org/10.1016/j.quascirev.2017.05.019.

Peltier, W.R., 1974. The impulse response of a Maxwell Earth. Rev. Geophys. 12 (4), 649. http://dx.doi.org/10.1029/RG012i004p00649.

Peltier, W.R., Argus, D.F., Drummond, R., 2015. Space geodesy constrains ice age terminal deglaciation: The global ICE-6G_C (VM5a) model: Global glacial isostatic adjustment. J. Geophys. Res. 120 (1), 450–487. http://dx.doi.org/10.1002/2014JB011176.

Pollard, O.G., Barlow, N.L.M., Gregoire, L.J., Gomez, N., Cartelle, V., Ely, J.C., Astfalck, L.C., 2023. Quantifying the uncertainty in the Eurasian ice-sheet geometry at the penultimate glacial maximum (marine isotope stage 6). Cryosphere 17 (11), 4751–4777. http://dx.doi.org/10.5194/tc-17-4751-2023.

Rohling, E.J., Hibbert, F.D., Williams, F.H., Grant, K.M., Marino, G., Foster, G.L., Hennekam, R., de Lange, G.J., Roberts, A.P., Yu, J., Webster, J.M., Yokoyama, Y., 2017. Differences between the last two glacial maxima and implications for ice-sheet, δ18O, and sea-level reconstructions. Quat. Sci. Rev. 176, 1–28. http://dx.doi.org/10.1016/j.quascirev.2017.09.009.

Rovere, A., Ryan, D.D., Vacchi, M., Dutton, A., Simms, A.R., Murray-Wallace, C.V., 2023. The World Atlas of last interglacial shorelines (version 1.0). Earth Syst. Sci. Data 15 (1), 1–23. http://dx.doi.org/10.5194/essd-15-1-2023.

Shakun, J.D., Lea, D.W., Lisiecki, L.E., Raymo, M.E., 2015. An 800-Kyr record of global surface ocean δ 18 O and implications for ice volume-temperature coupling. Earth Planet. Sci. Lett. 426, 58–68. http://dx.doi.org/10.1016/j.epsl.2015.05.042.

Shennan, I., Bradley, S.L., Edwards, R., 2018. Relative sea-level changes and crustal movements in Britain and Ireland since the last glacial maximum. Quat. Sci. Rev. 188, 143–159. http://dx.doi.org/10.1016/j.quascirev.2018.03.031.

Shennan, I., Bradley, S., Milne, G., Brooks, A., Bassett, S., Hamilton, S., 2006. Relative sea-level changes, glacial isostatic modelling and ice-sheet reconstructions from the British Isles since the last glacial maximum. J. Quat. Sci. 21 (6), 585–599. http://dx.doi.org/10.1002/jqs.1049.

Simon, K.M., Riva, R.E.M., 2020. Uncertainty estimation in regional models of long-term GIA uplift and sea level change: An overview. J. Geophys. Res. 125 (8), e2019JB018983. http://dx.doi.org/10.1029/2019JB018983.

Sobol', I.M., 1990. On sensitivity estimation for nonlinear mathematical models. Matematicheskoe modelirovanie 2 (1), 112–118.

Svendsen, J.I., Alexanderson, H., Astakhov, V.I., Demidov, I., Dowdeswell, J.A., Funder, S., Gataullin, V., Henriksen, M., Hjort, C., Houmark-Nielsen, M., Hubberten, H.W., Ingólfsson, Ó., Jakobsson, M., Kjær, K.H., Larsen, E., Lokrantz, H., Lunkka, J.P., Lyså, A., Mangerud, J., Matiouchkov, A., Murray, A., Möller, P., Niessen, F., Nikolskaya, O., Polyak, L., Saarnisto, M., Siegert, C., Siegert, M.J., Spielhagen, R.F., Stein, R., 2004. Late quaternary ice sheet history of Northern Eurasia. Quat. Sci. Rev. 23 (11–13), 1229–1271. http://dx.doi.org/10.1016/j.quascirev.2003.12.008.

Toucanne, S., Zaragosi, S., Bourillet, J., Cremer, M., Eynaud, F., Van Vliet-Lanoë, B., Penaud, A., Fontanier, C., Turon, J., Cortijo, E., 2009. Timing of massive 'Fleuve Manche' discharges over the last 350kyr: Insights into the European ice-sheet oscillations and the European drainage network from MIS 10 to 2. Quat. Sci. Rev. 28 (13–14), 1238–1256. http://dx.doi.org/10.1016/j.quascirev.2009.01.006.

Turner, F.E., Malagon Santos, V., Edwards, T.L., Slangen, A.B., Nicholls, R.J., Le Cozannet, G., O'Neill, J., Adhikari, M., 2023. Illustrative multi-centennial projections of global mean sea-level rise and their application. Earth's Future 11 (12), e2023EF003550. http://dx.doi.org/10.1029/2023EF003550.

van der Wal, W., Barnhoorn, A., Stocchi, P., Gradmann, S., Wu, P., Drury, M., Vermeersen, B., 2013. Glacial isostatic adjustment model with composite 3-D Earth rheology for Fennoscandia. Geophys. J. Int. 194 (1), 61–77. http://dx.doi.org/10.1093/gji/ggt099.

Waelbroeck, C., Labeyrie, L., Michel, E., Duplessy, J., McManus, J., Lambeck, K., Balbon, E., Labracherie, M., 2002. Sea-level and deep water temperature changes derived from benthic foraminifera isotopic records. Quat. Sci. Rev. 21 (1–3), 295–305. http://dx.doi.org/10.1016/S0277-3791(01)00101-9.

Zagwijn, W.H., 1983. Sea-Level Changes in the Netherlands during the Eemian, 62, (3), Koninklijk Nederlandsch Geologisch Mijnbouwkundig Genootschap, Haarlem, pp. 437–450.